Journal of the European Ceramic Society xxx (xxxx) xxx–xxx

Contents lists available at ScienceDirect

Journal of the European Ceramic Society

journal homepage: www.elsevier.com/locate/jeurceramsoc

Original Article

Order–disorder transition in the $Dy_{0.2}Sr_{0.8}CoO_{3-}\delta$ rare-earth cobalt oxide solid solutions: Structural and thermoelectric properties

Yu.S. Orlov[a,b,*], V.A. Dudnikov[a], S.N. Vereshchagin[c], M.N. Volochaev[a], S.Yu. Gavrilkin[d], A.Yu. Tsvetkov[d]

[a] Kirensky Institute of Physics, Federal Research Center KSC SB RAS, Krasnoyarsk, 660036, Russia
[b] Siberian Federal University, Krasnoyarsk, 660041, Russia
[c] Institute of Chemistry and Chemical Technology, Federal Research Center KSC SB RAS, Krasnoyarsk, 660036, Russia
[d] Lebedev Physical Institute, Moscow, 119991, Russia

ARTICLE INFO

Keywords:
Substituted rare-earth cobalt oxides
Thermoelectric oxide materials
Ordered and disordered states
Phase transition

ABSTRACT

By the example of the $Dy_{0.2}Sr_{0.8}CoO_{3-}\delta$ compound undergoing an order–disorder phase transition with increasing temperature, we demonstrate a significant dependence of the kinetic properties on the morphology of the internal spatially inhomogeneous structure, which forms in the sample depending on the rate of its transition from the high-temperature disordered cubic phase to the ground tetragonal ordered phase upon cooling. The results of transmission electron microscopy visualization of the spatially inhomogeneous state in the $Dy_{0.2}Sr_{0.8}CoO_{3-}\delta$ ceramic samples are presented and compared with the X-ray diffraction data.

1. Introduction

The development of alternative ways of energy conversion requires the search for new materials necessary for the practical implementation of these ways. Direct conversion of heat into electricity can be carried out in thermoelectric generators. Thermoelectric energy conversion is one of the ways to introduce energy-saving technologies and implement rational use of natural resources. For operation of thermoelectric generators, materials with high thermoelectric figure of merit or efficiency of conversion of thermal energy into electrical energy are necessary. In this connection, much attention was paid to solid-state thermoelectric converters.

The main problem hindering the development of this promising area of energy is that a number of very stringent and often mutually exclusive requirements are imposed on materials for thermoelectric devices. In particular, thermoelectrics should combine high electrical conductivity with low thermal conductivity. Important characteristics in the search for new thermoelectric materials, in addition to the Q factor, are such parameters as the absence of toxic elements, high chemical and temperature stability.

The application prospects of novel thermoelectric materials are determined by the success in optimizing their properties. At present, the main optimization tool is phonon engineering [1], which allows one to create narrow-gap semiconductors with the very low thermal conductivity via separation of structural fragments on the nanoscale. The promising substances for creating a new generation of thermoelectric materials include nanostructured materials or spatially inhomogeneous materials with nanometer inhomogeneities comparable in size with the characteristic electron or phonon wavelengths [2]. The ability to control chemical and physical structuring in the nanometer region is important for the development of high-performance thermoelectric materials [3]. The progress in this area was mainly made, as was mentioned above, by enhancing phonon scattering and, therefore, reducing the thermal conductivity of the lattice using either the design of interfacial structures at the nanometer or mesoscopic level [4–8] or the creation of multiscale hierarchical structures [9,10].

The $R_{1-x}M_xCoO_{3-}\delta$ rare-earth cobaltites (R and M are the rare-earth and alkaline-earth metals, respectively, and δ is the oxygen nonstoichiometry index) are unique materials that make it possible to implement all the main methods proposed for increasing the thermoelectric figure of merit of spatially inhomogeneous thermoelectric materials, including doped materials, solid solutions, and alloys. In addition, a feature of most complex cobalt oxides that clearly distinguishes them among orther strongly correlated transition metal oxides is their proximity to the spin crossover. This proximity results in fluctuations of the spin and orbital multiplicity of cobalt ions and provides an additional mechanism of electron and phonon scattering.

The disordered $R_{1-x}Sr_xCoO_{3-}\delta$ perovskites of rare-earth elements

* Corresponding author at: Kirensky Institute of Physics KSC SB RAS, 660036, Krasnoyarsk, Russia.
E-mail addresses: orlov@iph.krasn.ru, jso.krasn@mail.ru (Y.S. Orlov).

https://doi.org/10.1016/j.jeurceramsoc.2020.06.066
Received 7 April 2020; Received in revised form 23 June 2020; Accepted 26 June 2020

with a radius smaller than that of Nd^{3+} exist at high temperatures; at low temperatures, a structure with the ordered Sr^{2+} and R^{3+} cations and anionic vacancies is stable [11]. However, the disordered $R_{1-x}Sr_xCoO_{3-\delta}$ perovskites can be obtained in the form of metastable phases by quenching the high-temperature states [12].

Recently, we have found that, upon the transition from a layered tetragonal phase with the ordered distribution of Gd/Sr ions in cobaltite $Gd_{0.2}Sr_{0.8}CoO_{3-\delta}$ to a cubic phase with the random arrangement of Sr^{2+} and Gd^{3+} cations in the A sites of the crystal lattice, many physicochemical properties, including the value of oxygen nonstoichiometry and type of the ordering of oxygen vacancies [12,13], change. This affects the mobility of lattice oxygen/oxygen vacancies and, consequently, the oxygen-ion conductivity.

The other feature established by us is a noticeable temperature shift of the maximum on DSC curves with a change in the rate of cooling of the $Gd_{0.2}Sr_{0.8}CoO_{3-\delta}$ sample from high temperatures and a significant heating–cooling hysteresis [14]. This behavior is characteristic of the first-order phase transitions and indicates transformation of the material from disordered to ordered state through nucleation with intermediate formation of two-phase system. The formation of such a spatially inhomogeneous state can improve the thermoelectric properties, since it reduces the thermal conductivity due to the additional phonon scattering mechanism.

Understanding of the details of the order-disorder phase transition in perovskites and stabilization of the metastable disordered states is necessary for synthesis of the systems with a controlled ordering level. Such states often possess new properties atypical for conventional perovskites. In particular, the lead-containing perovskites (relaxors) have extremely high dielectric constants due to the existence of nano-ordered regions in a disordered matrix [15]. To date, a wealth of practical material on the physicochemical properties of ordered/disordered perovskites has been accumulated [16,17]; however, there has been a lack of studies on the mutual transformations of the structures. Scientific ideas about obtaining partially disordered polyphase metastable structures are also few in numbers. The aim of this work is to study the features of the process of ordering of Sr^{2+}/Dy^{3+} cations by the example of the order-disorder phase transition in the $Dy_{0.2}Sr_{0.8}CoO_{3-\delta}$ (DySC) system and its effect on the thermoelectric properties.

2. Experimental

Polycrystalline $Dy_{0.2}Sr_{0.8}CoO_{3-\delta}$ samples with a perovskite structure were obtained using a conventional ceramic technology from a stoichiometric mixture of the Co_3O_4 (99.7 %, metalsbasis), Dy_2O_3 (99.99 %, REO), and $SrCO_3$ (99.99 %, metalsbasis), oxides thoroughly grinded in an agate mortar with ethanol. The resulting mixture was pressed into disks and annealed at a temperature of 1473 K in a platinum crucible for 24 h in air with multiple repetitions of the grinding–calcination cycles. To form a tetragonal ordered structure of $Dy_{0.2}Sr_{0.8}CoO_{3-\delta}$ (DySC-ord) ceramic discs were cooled in air from 1473 K to room temperature at a rate of 2°/min. The disordered cubic $Dy_{0.2}Sr_{0.8}CoO_{3-\delta}$ modification (DySC-dis) was formed by quenching the ceramic disc from 1473 K in air; an estimated cooling rate at 1000 − 1300 K was about 3000°/min. The partially disordered $Dy_{0.2}Sr_{0.8}CoO_{3-\delta}$ compound was synthesized directly in the cell of a thermal analyzer (TG-DSC). To do that, monolithic ceramic fragments about 2 × 2 × 1 mm in size (a sample mass of ~22.4 mg) were heated to T = 1473 K at a rate of 10°/min in a flow of the 20 % O_2-Ar mixture; then, the temperature linearly decreased to T = 773 K at different rates (β = 10, 20, 50, and 99°/min). All the samples were kept at 773 K for 1 h to stabilize the oxygen content.

The oxygen content and nonstoichiometry index δ were determined by the mass loss (Δm,%) [18] using a Netzsch STA 449C analyzer equipped with an Aeolos QMS 403C mass spectrometer. The Δm value was measured during the reduction of the samples in a flow of the 5% H_2–Ar mixture upon heating to 1173 K at a rate of 10°/min under the assumption that cobalt is reduced to the metal state. The obtained δ values are given in Table 1.

Table 1
Oxygen nonstoichiometry index δ of the $Dy_{0.2}Sr_{0.8}CoO_{3-\delta}$ samples cooled from 1473 K at rates of β = 2–3000°/min.

Sample	β, °/min	δ
DySC-2, annealed	2	0.37(1)
DySC-10	10	0.33(1)
DySC-20	20	0.32(1)
DySC-50	50	0.30(1)
DySC-99	99	0.29(1)
DySC-3000, quenched	3000	0.27(1)

The X-ray diffraction analysis was made using a PANalyticalX'Pert PRO (CoKα) diffractometer in the 2θ range of 10–140°; the high-temperature shooting was performed in an Anton Paar HTK 1200 N high-temperature chamber. The results were processed using the full-profile analysis of polycrystalline substances by the Rietveld refinement [19] and the derivative difference minimization [20].

Structure investigations were carried out by scanning (SEM Hitachi SU3500 at 20 kV accelerating voltage) and transmission (TEM Hitachi HT7700 at 100 kV accelerating voltage) electron microscopy. For SEM studies surface of ceramic samples were prepared by 2 keV Ar^+ ion polishing (IV4Pro ion polishing system, Linda Technoorg). To visualize the spatially inhomogeneous state by transmission electron microscopy, ~50 nm-thick foils (lamellas) several microns in size were prepared from the ceramic samples using a focused ion beam system (FIB Hitachi FB2100) with following 2 keV Ar^+ ion polishing. The electron microscopy investigations were carried out on the equipment of Krasnoyarsk Regional Center of Research Equipment of Federal Research Center «Krasnoyarsk Science Center SB RAS».

The temperature dependences of thermoelectric parameters were obtained on a Quantum Design Physical Properties Measurement System (PPMS-9) equipped with a special module for this type of measurements at the Center for Collective Use of the Lebedev Physical Institute, Russian Academy of Sciences (Moscow). The precision of measurements is 2 % for electrical resistivity and 0.5 μV/K ± 5 % for thermopower.

3. Results and discussion

After slow cooling (annealing) of the Dy-Sr perovskite from 1473 K at a rate of 2°/min in a mixture of 20 % O_2-Ar and exposure at 773 K for 1 h to stabilize the oxygen content, the sample composition corresponded to the $Dy_{0.2}Sr_{0.8}CoO_{2.63}$ (δ = 0.37) formula and the structure, according to the X-ray diffraction data (Fig. 1a), was a tetragonal *I4/mmm* superstructure with the ordered Sr^{2+}/Dy^{3+} ions and anionic vacancies (Fig. 2a), similar to that described in [11].

The structure of the ordered $Dy_{0.2}Sr_{0.8}CoO_{2.63}$ perovskite is similar to the structure of double strontium cobaltites with rare-earth metals [11], in which the A cations are partially ordered in columns [17]. In this structure, there are three nonequivalent positions of the A cation (A1, A2, and A3 sites in Fig. 2a), two of which are only occupied by Sr^{2+} ions and the third one is filled by randomly selected Sr^{2+} or Dy^{3+} cations (Fig. 2a). The structure contains four nonequivalent oxygen positions (Fig. 2a, O1-O4 positions) and, according to the results of our investigations at T = 298 K, anionic vacancies in the samples are only localized in the O2 position (Fig. 2a, O2 positions are colored in yellow), which is consistent with the literature data [11].

In-situ high-temperature X-ray phase analysis of the similar $Gd_{0.2}Sr_{0.8}CoO_{2.63}$ compound performed by us in [14] has revealed that above 1373 K the superstructural reflections disappeared and a disordered nonstoichiometric cubic perovskite with the uniform random distribution of Sr/Gd cations and anion vacancies was formed, the

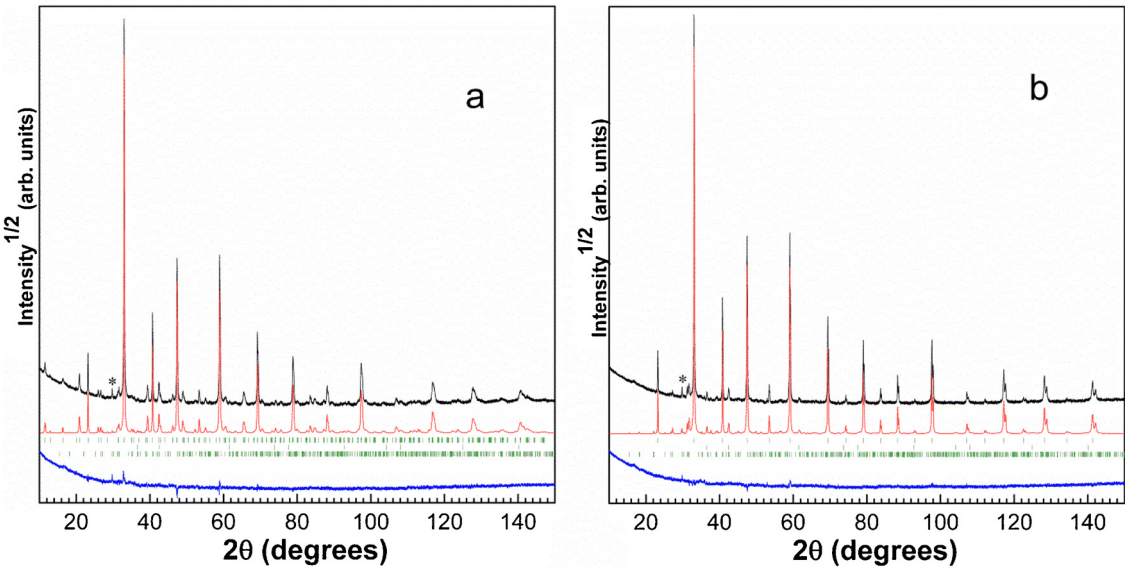

Fig. 1. Experimental (black line), calculated (red line), and difference (blue line) X-ray diffraction patterns after crystal structure refinement by the derivative difference minimization (DDM) for (a) the annealed (ordered) DySC-ord and (b) quenched (disordered) DySC-dis samples at room temperature. The calculated reflection positions are shown by strokes. The Cu K_β line of the main reflection is marked by the asterisk. (For interpretation of the references to colour in this figure legend, the reader is referred to the web version of this article).

composition of which at 1473 K corresponded to the formula $Gd_{0.2}Sr_{0.8}CoO_{2.51}$. Upon fast (at a rate of about 3000°/min) cooling from 1473 K, the Gd-Sr ceramic sample, retained a cubic *Pm3m* structure [14]. The obtained quenched metastable state remained unchanged in air at temperatures below 1073 K. A similar situation occurs for Dy-Sr perovskite: in Fig. 1b presents the X-ray diffraction pattern obtained at room temperature of a quenched and oxygen-stabilized Dy-Sr sample and corresponding to a *Pm3m* cubic structure with a uniform random distribution of Sr/Dy cations and anion vacancies (Fig. 2b).

Fig. 3 shows microphotographs of the annealed (ordered) $Dy_{0.2}Sr_{0.8}CoO_{2.63}$ perovskite surface. The surfaces of the quenched (disordered) $Dy_{0.2}Sr_{0.8}CoO_{2.73}$ sample and the samples obtained at intermediate cooling rates look similarly.

Ceramic grains from about 5 to 40 μm in size are clearly visible, from which ~ 50 nm thin foils (lamellas) of several microns in size were prepared using focused ion beam (FIB) for study using transmission electron microscopy (TEM). Figs. 4 and S1 show TEM images of the ordered (annealed) $Dy_{0.2}Sr_{0.8}CoO_{2.63}$ compound on different scales ((4) general view and (S1) high resolution (HREM)) and Figure S2 shows the image of the quenched sample. In the annealed sample, ordered domains with a layered tetragonal crystal structure (Fig. S1) and a characteristic size of up to ~100 nm (Fig. 4) are formed inside ceramic grains (Fig. 3). For clarity, half of the image in Fig. S1 is presented in the form corrected using Fourier filtering (Figs. S2 and S4 are similar).

In the quenched sample, the formation of a layered nanostructure was revealed (Fig. S2), which represents a three-dimensional domain texture in which domains of the ordered layered tetragonal phase with a characteristic size from 3 to 10 nm make right angles with each other. A very similar nanodomain structure was observed and described in detail in [21] for the stoichiometric $La_{0.5}Ba_{0.5}CoO_3$ perovskite and called pseudocubic by the authors because its X-ray diffraction pattern is very similar to the diffraction pattern of a true disordered cubic $La_{0.5}Ba_{0.5}CoO_3$ perovskite [21]. It is important that the X-ray diffraction patterns of the quenched and stabilized $Dy_{0.2}Sr_{0.8}CoO_{2.73}$ samples synthesized in this work (Fig. 1b) and of the $Gd_{0.2}Sr_{0.8}CoO_{2.73}$ samples prepared by us previously [14] that were obtained at room temperature and in-situ for the Gd-Sr perovskite in [14] at temperatures above 1373 K are almost identical. Thus, despite the high quenching rate (β = 3000°/min), it is impossible to freeze the completely disordered true cubic phase that exists at high (T > 1373 K) temperatures. Instead, a nanodomain structure is formed, which, as in [21], can be called pseudocubic. We have a striking example of the fact that the most complete description of the internal structure of perovskite solid solutions is provided by the combined use of the X-ray and electron microscopy methods.

As was shown in [22], the phase transition of the tetragonal $Gd_{0.2}Sr_{0.8}CoO_{3-}\delta$ perovskite with the ordered Sr^{2+}/Gd^{3+} cations to the disordered cubic modification, which occurs in the temperature range of 1331–1383 K, obeys the regularities characteristic of the blurred first-order phase transitions. The disordering of cations and oxygen vacancies occurs easily and does not depend on the heating rate; the state of the system during the disordering is controlled by the thermodynamic characteristics of the processes occurring in the crystal, rather than by the kinetics of formation and growth of new phase nuclei. In contrast to the order-disorder transition, the inverse process of the formation of an ordered tetragonal structure is controlled by the kinetic factors, including the nucleation and/or growth rates. Thus, cobaltites with different degrees of ordering should be obtained from a completely disordered perovskite (T > 1398 K for the investigated composition) by varying the cooling/annealing temperature conditions and the composition of gaseous media.

Figure S3 shows fragments of the X-ray diffraction patterns of the $Dy_{0.2}Sr_{0.8}CoO_{3-}\delta$ samples cooled at different rates β. Some superstructural reflections of the tetragonal phase (the red line in Fig. S3 coresponds to the annealed sample; β = 2°/min) are indexed. Figure S3b shows an enlarged region of the superstructural reflections [002] and [103]. One can clearly see a decrease in the intensity of superstructural reflections with an increase in the quenching rate. In Fig. 5, according to X-ray diffraction data, the dependence of the cell volume and the crystal lattice parameters of the cubic (a_p) and tetragonal ($a/2$, $c/4$) $Dy_{0.2}Sr_{0.8}CoO_{3-}\delta$ phases on the cooling rate β is plotted. At β ≥ 99°/min, the X-ray diffraction patterns are indexed in the cubic *Pm3m* syngony and, at β ≤ 50°/min, in the tetragonal *I4/mmm* one; at β = 50°/min, the parameters of the tetragonal phase satisfy the relation $a_p = a/2 = c/4$; i.e., despite the occurrence of superstructural reflections, the lattice expands uniformly in all the directions. The region β ≈ 20°/min is transitional, where the superstructural reflections become pronounced (Fig. S3) and the lattice expansion becomes anisotropic with a predominant increase in the parameter c: $a/2 < c/4$ (Fig. 5). For the annealed sample (β = 2°/min), we have c = 15.366(1) Å, which is

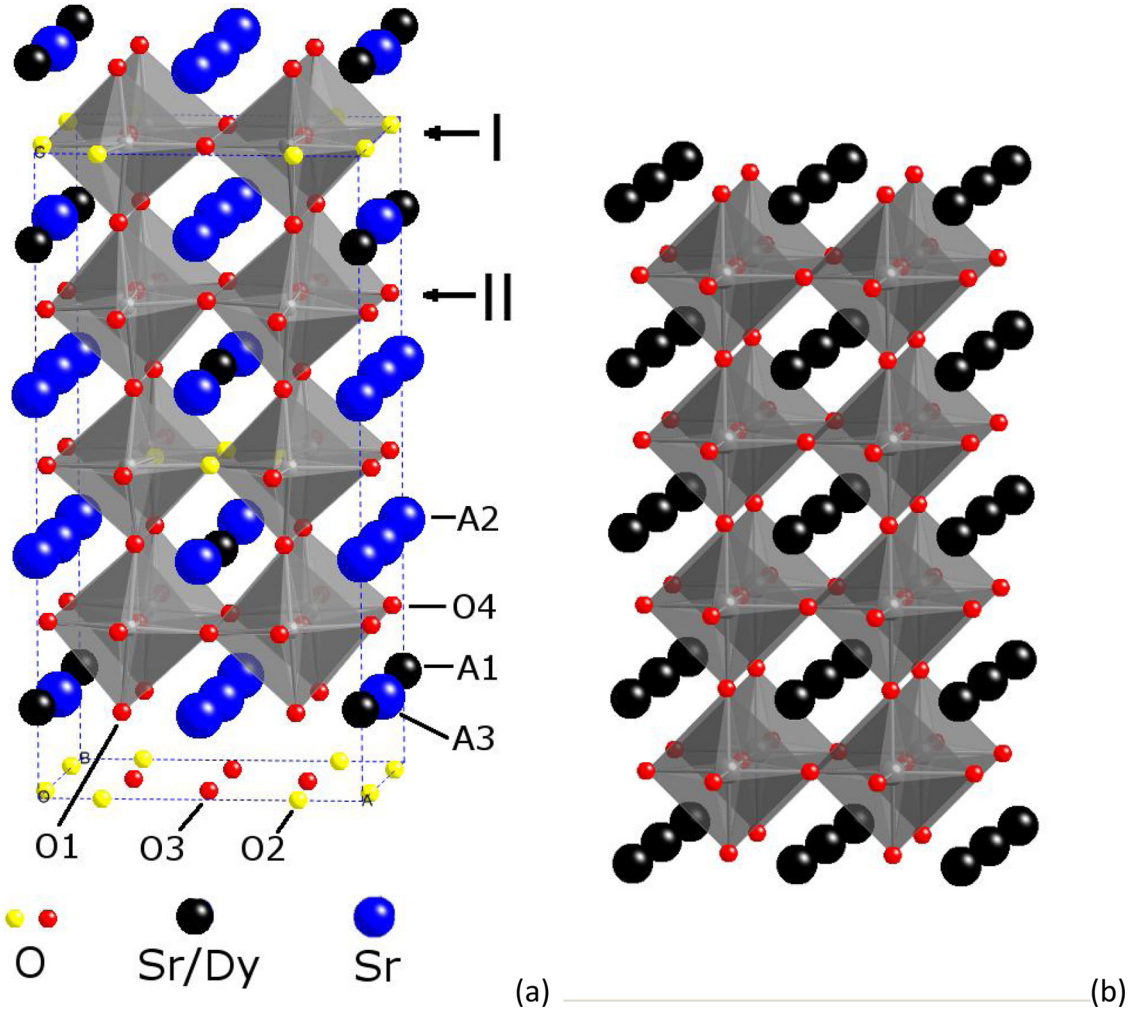

Fig. 2. (a) Tetragonal and (b) cubic structures of the $Dy_{0.2}Sr_{0.8}CoO_3.\delta$ perovskite. The octahedra correspond to Co^{3+} cations and the red and yellow spheres, to the position of O^{2-}/anion vacancies; the Sr^{2+} positions are shown in blue, the positions of R^{3+} cations are shown in black; and A1, A2, and A3 show three nonequivalent positions of the A cation. Four nonequivalent oxygen positions are marked by O1–O4. The $CoO_{4+}\delta$ layers with oxygen atoms randomly removed from the O2 positions and the CoO_6 layers are indicated by I and II, respectively. (For interpretation of the references to colour in this figure legend, the reader is referred to the web version of this article).

consistent with the electron microscopy data. In Figs. S1, S2, and S4, two red marks show the distance between the crystal structure layers, which corresponds to the parameter $c/2$, i.e., multiple of period of layers I or II with and without oxigen vacancies (Fig. 2a).

At present, we cannot unambiguously state whether the observed domains (Fig. S2) are fully or partially ordered. However, it is most likely that, with decreasing β, the degree of ordering of the Sr/Dy cations (the deviation from the random distribution of A cations over the A1–A3 sites, Fig. 2) increases. At low degrees of ordering, the induced stresses cause an increase in the lattice parameter a_p in the pseudocubic perovskite, while the coherence of the perpendicularly oriented domain walls is maintained (Fig. S2). As the β value decreases, the degree of ordering of the Sr/Dy cations increases, stresses in the lattice and its local distortions at the atomic level increase, and, in the cooling rate range of β = 20–50°/min, a kink related to the violation of the ratio $a_p = a/2 = c/4$ is observed in the V_c dependence (Fig. 5).

Figure S4 shows the HRTEM image of a sample cooled at a rate of 20°/min. In this case, ordered layered nanodomains are also observed (shown by the arrow), which still make right angles with each other and have a characteristic size significantly smaller than in the annealed sample (Fig. S1), but larger than in the quenched one (Fig. S2). Instead of the 3D texture of the pseudocubic perovskite formed by coherently conjugate nanodomains of the ordered (or partially ordered) phase, the formation of larger domains connected by blurred transition regions is observed. These regions most likely correspond to the incoherent/semi-coherent walls between the domains of the ordered tetragonal phase and represent structural defects, which can substantially change the properties of a solid (crystal). Thus, it can be expected that the cooling rate range β = 20–50°/min is optimal for obtaining a material with nanodomains of an ordered phase and a high concentration of domain walls with the short-range order violation and maximum stresses in the lattice.

According to the electron microscopy and X-ray diffraction data, the rare-earth cobalt oxide solid solutions can be the basis for creation of the multiscale spatially inhomogeneous materials with different spatial arrangements of the ordered state. The multiscale type of the structure suggests the existence of inhomogeneities with different sizes. In particular, in the annealed samples, inside ceramic grains 5–40 μm in size (Fig. 3), ordered domains (Fig. 4) with a layered tetragonal crystal structure (Fig. S1) and a characteristic size of approximately 20–100 nm form, inside of which, in turn, there is an atomic-scale disorder caused by the average arrangement of cations and anions in certain crystal lattice positions (Fig. 2a). In the quenched samples, a nanoscale pseudocubic structure is formed inside ceramic grains (Fig. S2), which is a three-dimensional nanodomain texture of coherently conjugated nanometer domains of an ordered (or partially ordered) phase with the

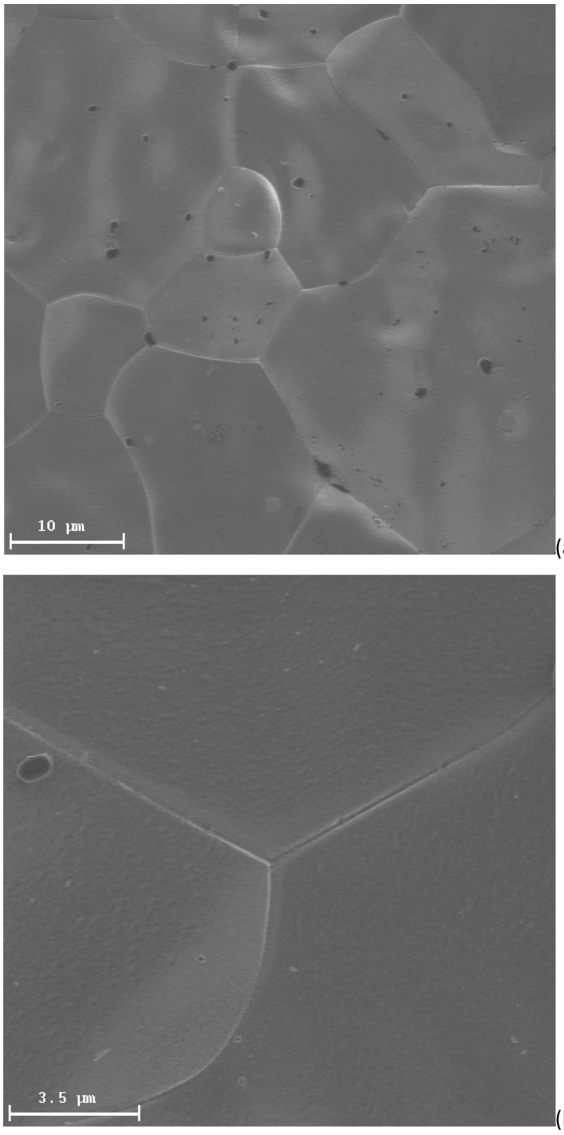

Fig. 3. Micrographs of the $Dy_{0.2}Sr_{0.8}CoO_{2.63}$ perovskite surface on different scales.

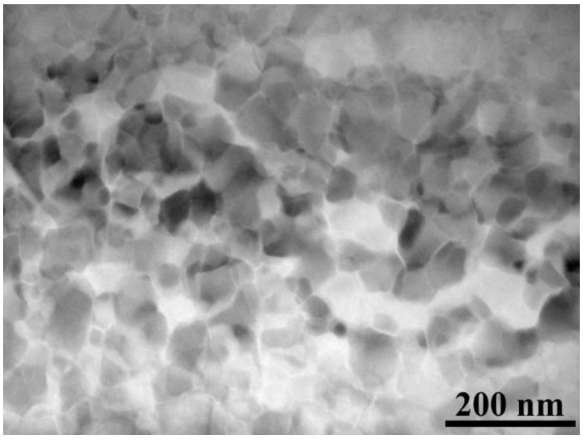

Fig. 4. Transmission electron microscopy images of the ordered (annealed) $Dy_{0.2}Sr_{0.8}CoO_{2.63}$ rare-earth cobalt oxide.

same atomic disorder related to the preferred arrangement of cations and anions (Fig. 2a). Finally, in the samples synthesized at an

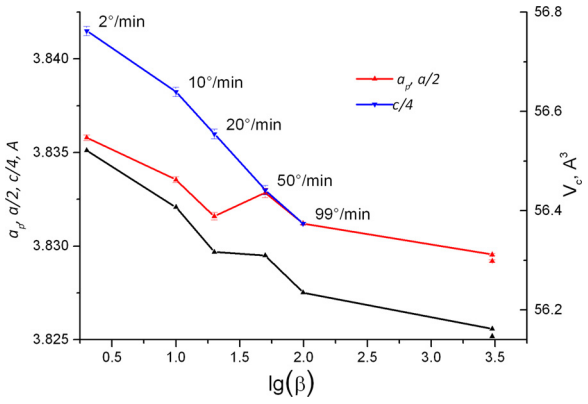

Fig. 5. Dependence of the cell volume (▲) and the parameters of the cubic (a_p) and tetragonal (a/2, c/4) $Dy_{0.2}Sr_{0.8}CoO_{3-}\delta$ phases on the cooling rate β. The oxygen content in the samples was stabilized at 773 K in a mixture of 20 % O_2-Ar (an oxygen partial pressure of 20.2 kPa).

intermediate quenching rate, a nanodomain texture of the tetragonal phase with the violation of a short-range order in the region of incoherent domain walls is formed inside the same ceramic grains (Fig. S4). It should be noted that the average size of the ceramic grains can be different for different grinding techniques used.

Fig. 6 presents the results of investigations of the temperature dependences of the kinetic coefficients, including Seebeck coefficient *S*

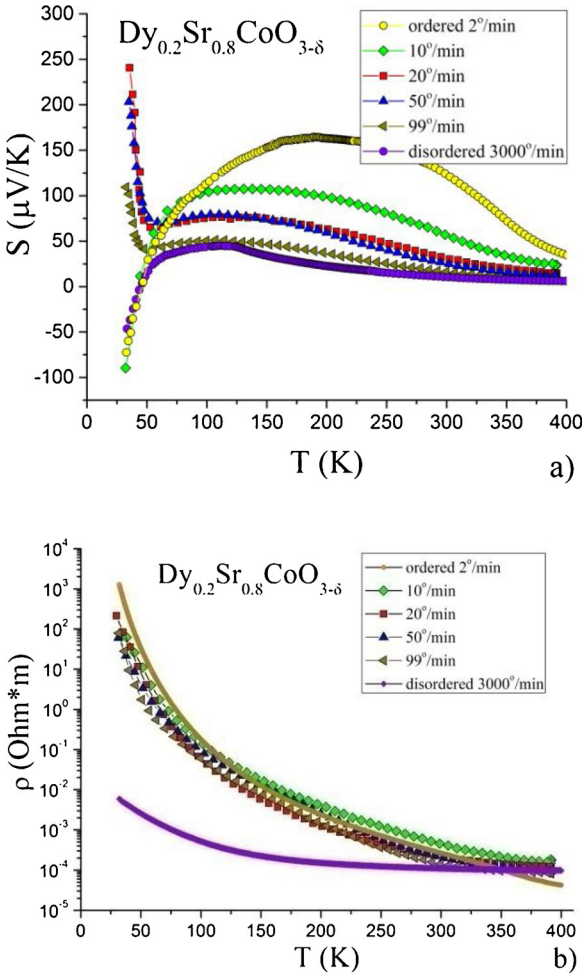

Fig. 6. Temperature dependences of the kinetic coefficients of the samples obtained at different cooling rates β: (a) Seebeck coefficient *S* and (b) electrical resistivity ρ.

and electrical resistivity ρ in the temperature range from 30 to 400 K for the samples obtained at different cooling rates β.

Due to the formation of the above-mentioned multiscale spatially inhomogeneous structure in the investigated samples, they exhibit different kinetic properties. A significant difference between samples with an intermediate cooling rate (β = 20, 50, 99°/min) from rapidly quenched and tempered is the behavior of their Seebeck coefficient S at $T \rightarrow 0$ (Fig. 6a), apparently due to the presence of disordered regions of interdomain boundaries (Fig. S4). So, if for the quenched and annealed samples the Seebeck coefficient changes sign and decreases sharply, taking negative values at low temperatures then the Seebeck coefficient of samples with an intermediate cooling rate does not change sign and sharply increases with decreasing temperature. It is worth noting that the behavior of the DySC-2 and DySC-10 samples is quite similar. In this paper we cannot give a full explanation of such an unusual behavior but we will try to bring some considerations on this subject and the necessary explanations to the results of the measurement (Fig. 6). It is well known that for intrinsic semiconductors the Seebeck coefficient is

inversely proportional to the temperature $\sim 1/T$, in doped semiconductors it is proportional to $\sim \ln (T^{3/2})$, and in metals and degenerate semiconductors it is directly proportional to the temperature $\sim T$ [23–27], i.e. in dielectrics and non-degenerate semiconductors Seebeck coefficient diverges at $T \rightarrow 0$. Makhan [28,29] has given an explanation of why in experiments for dielectrics and nondegenerate semiconductors instead of divergence the Seebeck coefficient vanishes in the low temperature limit. This is due to the "space-charge effects" [28,29]. We also observe the Seebeck coefficient vanishing at $T \rightarrow 0$ for samples with an intermediate cooling rate (the results of measurements at $T < 30$ K are not presented because of the high electrical resistance of the samples in this temperature range), but with increasing temperature the effect of space charge on the measurement of thermopower decreases and at $T > 30$ K we again observe the asymptotically correct (not masked by space charge effects) behavior of thermopower at low temperatures (Fig. 6a). Since the electrical resistance for the materials under study is quite large in the low-temperature range, it becomes possible to measure it at our installation at $T > 30$ K (Fig. 6b) therefore a reliable result of measuring the Seebeck coefficient the data obtained at $T > 30$ K (Fig. 6a) can be considered. But this is already enough to observe a contrast difference between samples obtained at an intermediate cooling rate from quenched and annealed (Fig. 6a). From electroneutrality condition we can conclude that for semiconductor $R_{1-x}M_xCoO_3$-δ compounds with an oxygen nonstoichiometry index of $\delta < 0.4$, the substitution of R^{3+} ions by M^{2+} ions leads to hole doping, and for $\delta > 0.4$ to electron doping. Thus, in the limit of low temperatures substituted rare-earth cobalt oxides with an oxygen nonstoichiometry index of $\delta < 0.4$ and $\delta > 0.4$ should have asymptotically different in sign behavior of the Seebeck coefficient [28,29]. We have already noted that in-situ high-temperature X-ray phase analysis performed for a similar compound $Gd_{0.2}Sr_{0.8}CoO_3$-δ in our work [14] showed that a disordered nonstoichiometric true cubic perovskite with uniform random distribution of Sr/Gd cations and anion vacancies is formed above 1373 K, whose composition at 1473 K corresponds to the formula $Gd_{0.2}Sr_{0.8}CoO_{2.51}$ and therefore has the electron type of conductivity ($\delta > 0.4$). In the present work the in-situ measurements for $Dy_{0.2}Sr_{0.8}CoO_3$-δ were not performed at high temperatures but we have reason to believe that a similar situation also holds for $Dy_{0.2}Sr_{0.8}CoO_3$-δ. Despite the fact that a truly cubic disordered phase exists only at high temperatures it seems that the disordered regions of the interdomain boundaries in samples with an intermediate cooling rate (Fig. S4) have much in common with this phase. We assume that having the same nonstoichiometry the interdomain boundaries exhibit the electron type of conductivity in contrast to the domains themselves with the hole type conductivity. This accounts for a sharp increase in the Seebeck coefficient of samples with an intermediate cooling rate at low temperatures (Fig. 6a) and their difference from quenched and annealed samples.

To verify our assumption we synthesized a sample of

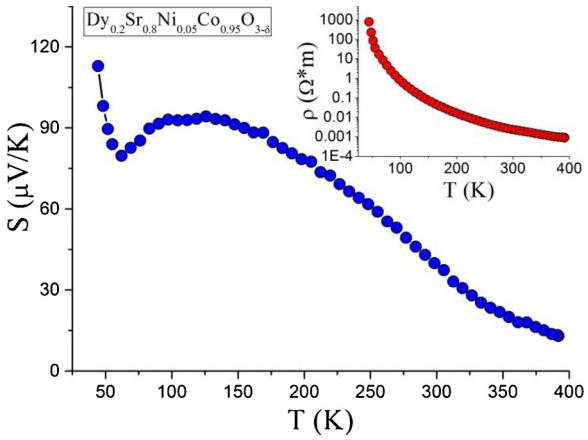

Fig. 7. Temperature dependence of the Seebeck coefficient S and electrical resistivity ρ (inset) of $Dy_{0.2}Sr_{0.8}Co_{0.95}Ni_{0.05}O_3$-δ solid solution.

$Dy_{0.2}Sr_{0.8}Co_{0.95}Ni_{0.05}O_3$-δ with a small electron doping. Fig. 7 shows the temperature dependence of its Seebeck coefficient S and electrical resistivity ρ (inset). It can be seen that the low-temperature behavior of DySC-20, 50, 99 samples corresponds to the behavior of the $Dy_{0.2}Sr_{0.8}Co_{0.95}Ni_{0.05}O_3$-δ solid solution.

Thus without explicit electron doping and choosing only the cooling rate of the $Dy_{0.2}Sr_{0.8}CoO_3$-δ perovskite which undergoes the order-disorder structural transition we managed to change the conductivity type which is noticeably manifested in the behavior of the Seebeck coefficient at low temperatures.

4. Conclusions

Along with varying the nature of cations in the $R_{1-x}M_xCoO_3$-δ rare-earth cobalt oxide solid solutions with a perovskite structure and their distribution over the crystal lattice, a significant change in their characteristics or even the occurrence of fundamentally new properties can be obtained via the creation of domains of different degrees of ordering and/or phase nanoinclusions in the perovskite array. The formation of metastable structures of local inhomogeneities in a solid can be expected in the region of phase transitions. By the example of the $Dy_{0.2}Sr_{0.8}CoO_3$-δ compound undergoing an order–disorder phase transition with increasing temperature, we demonstrate a significant dependence of the kinetic properties on the morphology of the internal spatially inhomogeneous structure, which forms in the sample depending on the rate of its transition from the high-temperature disordered cubic phase to the ground tetragonal ordered phase upon cooling (on its quenching rate). For this purpose, we synthesized a series of oxygen-stabilized samples at different rates of cooling from high temperatures. It was found that, in the tempered sample (the cooling rate is 2°/min) the ordered regions with a layered tetragonal crystal structure and a characteristic size from 40 to 100 nm are formed inside ceramic grains from 5 to 40 μm in size. In the quenched sample (the cooling rate is 3000°/min), instead of the expected completely disordered metastable cubic phase, a nanoscale layered structure or the so-called pseudocubic structure (see Section 3) with a characteristic size of 4–10 nm was formed. Finally, choosing an intermediate cooling rate (β ≈ 20°/min), we managed to synthesize the samples with a nanodomain texture of the tetragonal phase and short-range order violations in the region of incoherent domain walls. In the temperature range from 30 to 400 K, the thermoelectric properties of all the synthesized samples were studied. In the low-temperature region a significant difference of Seebeck coefficient of samples obtained at an intermediate cooling rate from quenched and annealed samples was found. Due to the high electrical resistance at low temperatures all samples have insignificant thermoelectric figure of merit ZT; however, the investigated method

can be used to improve the thermoelectric parameters of another even more promising thermoelectrics that experience the first-order order-disorder phase transition and have the lower electrical resistivity.

Declaration of Competing Interest

The authors declare that they have no known competing financial interests or personal relationships that could have appeared to influence the work reported in this paper.

Acknowledgements

The authors are grateful to Professor S.G. Ovchinnikov for discussing the results and comments made.

This study was supported by the Russian Science Foundation, project no. 19-72-00097.

Appendix A. Supplementary data

Supplementary material related to this article can be found, in the online version, at doi:https://doi.org/10.1016/j.jeurceramsoc.2020.06.066.

References

[1] A. Balandin, D. Nika, Phononics in low-dimensional materials, Mater. Today 15 (2012) 266–275, https://doi.org/10.1016/S1369-7021(12)70117-7.
[2] Aleksei V. Dmitriev, Igor P. Zvyagin, Current trends in the physics of thermoelectric materials, Physics-Uspekhi 53 (2010) 789–803, https://doi.org/10.3367/UFNe.0180.201008b.0821.
[3] M.S. Dresselhaus, G. Chen, M.Y. Tang, R.G. Yang, H. Lee, D.Z. Wang, Z.F. Ren, J.-P. Fleurial, P. Gogna, New directions for low-dimensional thermoelectric materials, Adv. Mater. 19 (2007) 1043–1053, https://doi.org/10.1002/adma.200600527.
[4] M. Zhou, J.F. Li, T. Kita, Nanostructured $AgPb_mSbTe_{m+2}$ system bulk materials with enhanced thermoelectric performance, J. Am. Chem. Soc. 130 (2008) 4527–4532, https://doi.org/10.1021/ja7110652.
[5] Y.J. Hu, L.P. Zeng, A.J. Minnich, M.S. Dresselhaus, G. Chen, Spectral mapping of thermal conductivity through nanoscale ballistic transport, Nat. Nanotechnol. 10 (2015) 701–706, https://doi.org/10.1038/nnano.2015.109.
[6] Wen-Yu Zhao, Zhu Liang, Ping Wei, Jian Yu, Qing-Jie Zhang, Guo-Sheng Shao, Enhanced thermoelectric performance via randomly arranged nanopores: excellent transport properties of $YbZn_2Sb_2$ nanoporous materials, Acta Mater. 60 (2012) 1741–1746, https://doi.org/10.1016/j.actamat.2011.11.056.
[7] Chenguang Fu, Shengqiang Bai, Yintu Liu, Yunshan Tang, Lidong Chen, Xinbing Zhao, Tiejun Zhu, Realizing high figure of merit in heavy-band *p*-type half-Heusler thermoelectric materials, Nat. Commun. 6 (2015) 8144, https://doi.org/10.1038/ncomms9144.
[8] Yubo Luo, Junyou Yang, Qinghui Jiang, Weixin Li, Dan Zhang, Zhiwei Zhou, Yudong Cheng, Yangyang Ren, Xu He, Progressive regulation of electrical and thermal transport properties to high-performance $CuInTe_2$ thermoelectric materials, Adv. Energy Mater. 6 (2016) 1600007, https://doi.org/10.1002/aenm.201600007.
[9] Kanishka Biswas, Jiaqing He, Ivan D. Blum, Chun-I. Wu, Timothy P. Hogan, David N. Seidman, Vinayak P. Dravid, Mercouri G. Kanatzidis, High-performance bulk thermoelectrics with all-scale hierarchical architectures, Nature 489 (2012) 414–418, https://doi.org/10.1038/nature11439.
[10] H.J. Wu, L.-D. Zhao, F.S. Zheng, D. Wu, Y.L. Pei, X. Tong, M.G. Kanatzidis, J.Q. He, Broad temperature plateau for thermoelectric figure of merit $ZT > 2$ in phase-separated $PbTe_{0.7}S_{0.3}$, Nat. Commun. 5 (2014) 4515, https://doi.org/10.1038/ncomms5515.
[11] M. James, D. Cassidy, D.J. Goossens, R.L. Withers, The phase diagram and tetragonal superstructures of the rare earth cobaltate phases $Ln_{1-x}Sr_xCoO_3.\delta$ (Ln = La^{3+}, Pr^{3+}, Nd^{3+}, Sm^{3+}, Gd^{3+}, Y^{3+}, Ho^{3+}, Dy^{3+}, Er^{3+}, Tm^{3+} and Yb^{3+}), J. Solid State Chem. 177 (2004) 1886–1895, https://doi.org/10.1016/j.jssc.2004.01.012.
[12] S.N. Vereshchagin, L.A. Solovyov, E.V. Rabchevskii, V.A. Dudnikov, S.G. Ovchinnikov, A.G. Anshits, Methane oxidation over A-site ordered and disordered $Sr_{0.8}Gd_{0.2}CoO_3.\delta$ perovskites, Chem. Commun. 50 (2014) 6112–6115, https://doi.org/10.1039/C4CC00913D.
[13] V.A. Dudnikov, Yu.S. Orlov, N.V. Kazak, A.S. Fedorov, L.A. Solov'yov, S.N. Vereshchagin, A.T. Burkov, S.V. Novikov, S.Yu. Gavrilkin, S.G. Ovchinnikov, Effect of *A*-site cation ordering on the thermoelectric properties of the complex cobalt oxides $Gd_{1-x}Sr_xCoO_3.\delta$ (x = 0.8 and 0.9), Ceram. Int. 44 (2018) 10299–10305, https://doi.org/10.1016/j.ceramint.2018.03.037.
[14] V.A. Dudnikov, Yu.S. Orlov, S.Yu. Gavrilkin, M.V. Gorev, S.N. Vereshchagin, L.A. Solovyov, N.S. Perov, S.G. Ovchinnikov, Effect of Gd and Sr ordering in A sites of doped $Gd_{0.2}Sr_{0.8}CoO_{3-}\delta$ perovskite on its structural, magnetic, and thermodynamic properties, J. Phys. Chem. C 120 (2016) 13443–13449, https://doi.org/10.1021/acs.jpcc.6b04810.
[15] A.S. Bhalla, R. Guo, R. Roy, The perovskite structure – a review of its role in ceramic science and technology, Mat. Res. Innov. 4 (2000) 3–26, https://doi.org/10.1007/s100190000062.
[16] R. Liu, Y. Xuan, Y.Q. Jia, Ordering and disordering in (A'A")(B'B")O_3-type perovskite compounds, Mater. Chem. Phys. 57 (1998) 81–85.
[17] G. King, P.M. Woodward, Cation ordering in perovskites, J. Mater. Chem. 20 (2010) 5785–5796, https://doi.org/10.1039/B926757c.
[18] K. Conder, E. Pomjakushina, A. Soldatov, E. Mitberg, Oxygen content determination in perovskite-type cobaltates, Mater. Res. Bull. 40 (2005) 257–263, https://doi.org/10.1016/j.materresbull.2004.10.009.
[19] H. Reitveld, A profile refinement method for nuclear and magnetic structures, J. Appl. Crystallogr. 2 (1969) 65–71, https://doi.org/10.1107/S0021889869006558.
[20] L.A. Solovyov, Full-profile refinement by derivative difference minimization, J. Appl. Crystallogr. 37 (2004) 743–749, https://doi.org/10.1107/S0021889804015638.
[21] Eeva-Leena Rautama, Philippe Boullay, Asish K. Kundu, Vincent Caignaert, Valérie Pralong, Maarit Karppinen, Bernard Raveau, Cationic ordering and microstructural effects in the ferromagnetic perovskite $La_{0.5}Ba_{0.5}CoO_3$: impact upon magnetotransport properties, Chem. Mater. 20 (2008) 2742–2750, https://doi.org/10.1021/cm703314p.
[22] Sergei N. Vereshchagin, Vyacheslav A. Dudnikov, Leonid A. Solovyov, DSC + TG and XRD study of order-disorder transition in nonstoichiometric Sr-Gd-Cobaltate, J. Sib. Fed. Univ. Chem. 3 (2016) 326–336, https://doi.org/10.17516/1998-2836-2016-9-3-326-336.
[23] Charles Kittel, Introduction to Solid State Physics, John Wiley & Sons, Inc, 2005.
[24] K.V. Shalimova, Physics of Semiconductors, Energoatomizdat, Moscow, 1985.
[25] V.L. Bonch-Bruevich, S.G. Kalashnikov, Fizika poluprovodnikov, Nauka, Moscow, 1977 (a) V.L. Bonch-Bruevich and S.G. Kalashnikov. Semiconductors Physics, Moscow, Science, 1977..
[26] A. Anselm, Introduction to Semiconductor Theory, Mir Publishers, Moscow, 1981.
[27] A.F. Ioffe, Semiconductor Thermocouples [in Russian], Soviet Academy of Sciences Press, Leningrad, 1960.
[28] G.D. Mahan, The low-temperature seebeck coefficient in insulators, J. Electron. Mater. 44 (2015) 431–434, https://doi.org/10.1007/s11664-014-3492-8.
[29] G.D. Mahan, The seebeck coefficient of insulators: electrochemical potential, J. Electron. Mater. 45 (2016) 1257–1259, https://doi.org/10.1007/s11664-015-3986-z.